Effect of Radial Temperature Profiles on Yields in Steam Cracking

K. M. Van Geem, G. J. Heynderickx, and G. B. Marin
Laboratorium voor Petrochemische Techniek, Ghent University, B-9000 Gent, Belgium

Radial temperature profiles during steam cracking result in radial nonuniformities in the product yields due to radial variations in the concentration of the radicals. The effect of using a 1-D or a 2-D reactor model on the calculated product yields is evaluated for the cracking of ethane. With a 2-D reactor model the simulated ethylene yield decreases. Ethylene formed at the high-temperature zone near the hot wall diffuses to the center where secondary reactions are favored, generating C_3 and C_4 olefins. This effect is confirmed by the calculation of a reactor of a Kellogg Millisecond Furnace. In this small-diameter reactor the 1-D behavior is more pronounced, resulting in higher ethylene yields at comparable conversions. The effect of the radial gradients on the coking rate calculated with a fundamental kinetic coking model based on elementary reaction steps is even more pronounced. Only when the coke model is coupled to a 2-D reactor model, a good agreement with the reference data is observed. In order to obtain accurate simulation results the more detailed 2-D reactor model is required, even if this increases the computational effort. © 2004 American Institute of Chemical Engineers *AIChE J,* 50: 173–183, 2004

Keywords: thermal cracking, two dimensional reactor model, simulation, coke formation, ethune cracking

Introduction

Tubular reactors are used in industry for important processes such as steam cracking and polymerization. Their analysis and design is frequently based on 1-dimensional models, that is, considering gradients only in the axial direction. Semiempirical correlations can approximate the average of radial concentration and temperature profiles from more-dimensional models (Sundaram and Froment, 1979), but do not provide any information on the importance and consequences of the nonuniformities for the reactor performance. The latter is of particular importance for the endothermic steam-cracking process. The trend toward high-severity cracking (Plehiers and Froment, 1991) demands higher heat fluxes, higher process-gas temperatures, and shorter residence times. Higher heat fluxes amplify the radial temperature gradients and make the 1-dimensional plug-flow model insufficient (Froment, 1992). Furthermore, a radial temperature gradient implies that the conditions prevailing at the process gas–coke interface on the one hand, and the conditions in the center of the reactor coil on the other hand may differ appreciably (De Saegher, 1996). Coke formation at the interface conditions (Sundaram et al., 1981) or at averaged conditions as calculated with a 1-dimensional model will differ. It was shown before (Heynderickx et al., 1992) that circumferential nonuniformities in flux and temperature, due to the shadow effects in the furnace, also result in nonuniform coking rates and coke layers. The radial temperature profile can have a significant effect on the calculated reactant concentrations and more in particular on those of the gas-phase radicals at the internal wall of the reactor tubes (Reyniers et al., 1994). The implementation of more dimensional models for complex reactions in a tubular reactor seems to be inevitable. Sundaram and Froment (1979, 1980) coupled a global kinetic model for the cracking of ethane to a two-dimensional (2-D) reactor model. Their results confirm the existence of important radial-temperature gradients. For molecular species, on the other

Correspondence concerning this article should be addressed to G. B. Marin at guy.marin@rug.ac.be.

hand, they found that radial-concentration gradients are less important. Valenyi et al. (1991) and Fagley (1992) proposed a 2-D model for the cracking of ethane in a tubular reactor with laminar flow, using the simulation packet PHOENICS to solve the 2-D mass, heat, and momentum balances. The kinetic model consisted of three reactions between five molecular species. Radial temperature differences up to 200 K were found, as were important radial molecular concentration gradients. No radical species were considered by any of these authors.

In this article, the cracking of ethane in a tubular reactor is simulated both with a 1-D and a 2-D reactor model. Both reactor models are coupled to a radical kinetic model for the cracking of naphtha and ethane. It consists of 60 molecular and 68 radical species and more than 1,200 reactions (Clymans and Froment, 1984). For ordinary tubular reactors a 2-D model is sufficient because of axial symmetry, but more complex geometries such as internally finned cracking coils demand a 3-D reactor model (De Saegher et al., 1996). The effect of the radial temperature and concentration profiles on the conversion and the product distribution is studied. Also the effect of these radial gradients on the coking rate is investigated. The results obtained with a coke-formation model based on elementary reactions (Wauters and Marin, 2001), coupled to a 1-D and 2-D reactor model, are compared with reference data. The effect on the calculated run length of the reactor is determined.

Procedures

The 1-D reactor model

The steady-state continuity equation for a component j in the process-gas mixture over an infinitesimal volume element with cross-sectional surface area, Ω, circumference ω, and length dz is

$$\frac{dF_j}{dz} = \left(\sum_{k=1}^{n_r} v_{kj} r_k \right) \Omega \tag{1}$$

The energy equation is given by

$$\sum_j F_j c_{pj} \frac{dT}{dz} = \omega q + \Omega \sum_k r_k (-\Delta H_k) \tag{2}$$

To calculate the wall temperature based on the process-gas temperature, the internal heat-transfer coefficient is calculated from the Dittus-Boelter equation

$$Nu = 0.023 Re^{0.8} Pr^{0.4} \tag{3}$$

The pressure equation accounting for friction and changes in momentum is given by

$$-\frac{dp_t}{dz} = \alpha \left(\frac{2f}{d_t} + \frac{\zeta}{\pi r_b} \right) \rho_g u^2 + \alpha \rho_g u \frac{du}{dz} \tag{4}$$

The boundary conditions for the 1-D problem at the inlet ($z = 0$) are

$$T = T_0 \qquad C_j = C_{j0} \qquad p = p_0$$

The process-gas temperature profile, conversion, and concentration profiles can be calculated based on an imposed heat-flux profile or external tube-skin temperature profile. In this article, calculations were performed using a heat-flux profile.

Integration of the continuity equations results in the concentration profiles of all the involved components. These equations form a set of stiff ordinary differential equations, that is, the local eigenvalues differ by several orders of magnitude. In practice, the concentration changes of the radicals occur on a much smaller time scale than that of the molecules. Therefore, an algorithm developed specifically for radical reaction networks has been employed (Dente and Ranzi, 1979).

The 2-D reactor model

The 2-D reactor model is based on a 2-D velocity vector. A mass balance for a component j over an annulus with height dz, internal radius r, and external radius $r + dr$ leads to the continuity equation for this component j in the process-gas mixture (Bird et al., 2001; Froment and Bischoff, 1990)

$$\frac{\partial}{\partial z}\left(u_z \frac{C_j}{\rho_g} \right) + \frac{1}{r}\frac{\partial}{\partial r}\left(r u_r \frac{C_j}{\rho_g} \right) - \frac{1}{r}\frac{\partial}{\partial r}\left(r \epsilon_D \rho_g \frac{\partial}{\partial r}\frac{C_j}{\rho_g} \right) - \sum_k v_{kj} r_k = 0 \tag{5}$$

Correspondingly, an energy balance leads to the energy equation

$$\frac{\partial}{\partial z}(u_z H) + \frac{1}{r}\frac{\partial}{\partial r}(r u_r H) - \frac{1}{r}\frac{\partial}{\partial r}\left(r \epsilon_H \frac{\partial T}{\partial r} \right) - \frac{1}{r}\frac{\partial}{\partial r}\left(r \sum_j H_j \epsilon_D \rho_g \frac{\partial}{\partial r}\frac{C_j}{\rho_g} \right) = 0 \tag{6}$$

Equation 6 considers heat transport and reaction simultaneously. The latter implies a good estimation of the simulated wall temperature. The last term in Eq. 6 is referred to as the interdiffusional energy flux by Bird et al. (2001). The origin of this term is the diffusion of chemical species. Explicitly introducing the reaction enthalpy in Eq. 6 results in Eq. 7

$$u_z c_p \frac{\partial T}{\partial z} + \left[u_r c_p - \epsilon_D \rho_g \sum_j (c_{pj}) \frac{\partial}{\partial r}\left(\frac{\partial_j}{\rho_g} \right) \right] \frac{\partial T}{\partial r} = \sum_k (-\Delta H_k) r_k \tag{7}$$

Radial pressure gradients are neglected and, hence, Eq. 4 is retained.

In the model equations no terms regarding coke layer thickness have been added, because the calculations are performed for the initial coke formation rate.

For the axial velocity component u_z the von Karman profile (Davies, 1972) is used. Three zones are considered over the entire tube length: a laminar, a turbulent and a transition zone.

In each zone the axial velocity is calculated using a different expression. In the laminar zone

$$\frac{u_z}{u_*} = \frac{\epsilon}{\epsilon_*} \quad \text{with} \quad u_* = \sqrt{\tau_w/\rho_g} \quad \text{and} \quad \epsilon_* = \nu/u_*. \tag{8}$$

In the transition zone

$$\frac{u_z}{u_*} = -3.05 + 5 \ln\left(\frac{\epsilon}{\epsilon_*}\right) \tag{9}$$

In the turbulent zone

$$\frac{u_z}{u_*} = 5.5 + 2.5 \ln\left(\frac{\epsilon}{\epsilon_*}\right) \tag{10}$$

After calculating the axial velocity profile according to Eqs. 8, 9, and 10, the radial component of the velocity u_r can be deduced from the total mass balance

$$\frac{\partial}{\partial z}(u_z \rho_g) + \frac{1}{r}\frac{\partial}{\partial r}(r u_r \rho_g) = 0 \tag{11}$$

The turbulent conductivity and diffusivity are calculated based on the correlation of Reichardt, corrected by Cebeci (Sundaram, 1977). The parameters have been further adjusted by Sundaram and Froment (1979). In Eqs. 12 and 13 the expressions for the turbulent conductivity ϵ_H and the turbulent diffusivity ϵ_D are given

$$\epsilon_H = \lambda_m[1 + c_3 Re^{c_1} Pr^{c_2}(1 + 2x^2)(1 - x^2)(1 - e^a) \times (1 - e^{-a\sqrt{Pr}/b})] \tag{12}$$

$$\epsilon_D = D_m[1 + c_3 Re^{c_1} Sc^{c_2}(1 + 2x^2)(1 - x^2) \times (1 - e^a)(1 - e^{-a\sqrt{Pr}/b})] \tag{13}$$

where x represents the normalized radius, $c_1 = 0.828664$, $c_2 = 0.944067$, $c_3 = 0.020530$, and the following expressions hold for a and b

$$a = (1 - x)\left(\frac{Re}{2}\right)\sqrt{\frac{f}{2}}$$

$$b = 34.96 + 28.79 \log(Pr) + 33.95 \log^2(Pr) + 6.33 \log^3(Pr) - 1.186 \log^4(Pr)$$

The Fanning friction factor is obtained from the Prandtl equation

$$\sqrt{f} = \frac{1}{r \log(Re\sqrt{f}) - 0.4} \tag{14}$$

In the laminar zone near the reactor wall, the conductivity equals the molecular conductivity, λ_m, and the diffusivity equals the molecular diffusion coefficient, D_m.

The boundary conditions for the 2-D problem are:

- In the center of the tube ($r = 0$)

$$\frac{\partial T}{\partial r} = 0 \qquad u_r = 0 \qquad \frac{\partial}{\partial r}\left(\frac{C_j}{\rho_g}\right) = 0$$

- At the inner reactor wall ($r = R$)

$$\epsilon_D \rho_g \frac{\partial}{\partial r}\left(\frac{C_j}{\rho_g}\right) = \frac{r_{c,j}}{M_j}.$$

- At the inlet ($z = 0$)

$$T = T_0 \qquad C_j = C_{j0} \qquad p = p_0$$

The axial heat profile is imposed at the inner wall ($r = R$)

$$\frac{\partial T}{\partial r} = \frac{q}{\epsilon_H} \tag{15}$$

This heat flux profile can be determined by calculating the radiative heat transfer in the furnace (Heynderickx and Froment, 1998). Circumferential nonuniformities due to the shadow effect in the furnace are not taken into account. The differential equations (Eqs. 5 and 7) are solved via a finite difference method. The Cranck-Nicholson method is used to calculate the differential variations in the axial direction. The differential variations in the radial direction are approximated by the second order differential of the Lagrange polynomial. For the application of the integration procedure a number of grid points has to be defined. Because of the steep gradients near the wall, a sufficiently small step size is required in that zone. The step size was varied according to a geometric progression: coarse in the core and fine near the wall. The set of differential equations for a specific variable in a radial section divided in n gridpoints i can then be rewritten in a tridiagonal format. For the concentration of component j, Eq. 16 is obtained

$$\begin{pmatrix} b_1 & d_1 & 0 & \cdots & 0 & 0 & 0 \\ a_2 & b_2 & d_2 & \cdots & 0 & 0 & 0 \\ \cdots & & & & & & \\ 0 & 0 & 0 & \cdots & 0 & a_n & b_n \end{pmatrix} \begin{pmatrix} C_{j,1} \\ C_{j,2} \\ \vdots \\ C_{j,n} \end{pmatrix} = \begin{pmatrix} e_1 \\ e_2 \\ \vdots \\ e_n \end{pmatrix} \tag{16}$$

This set of equations is solved simultaneously by the Thomas algorithm.

The implementation of a kinetic model based on a radical reaction mechanism again results in a stiff set of differential equations. The pseudo-steady-state approximation (PSSA) for the radicals cannot be used because it transforms the continuity equations for the radicals into algebraic equations. This makes it impossible to take the effect of the diffusion of radicals from neighboring zones into account, which requires a differential equation. Therefore a special solution method is used. An

element, e_i, on the righthand side of Eq. 16 contains the reaction rates calculated with the applied kinetic model. It is convenient to separate this contribution into two parts, one describing the cumulative rate of formation of the jth component by all reactions forming this component and the other describing the cumulative rate of disappearance of the same component

$$\sum_k \nu_{kj} r_k = \sum_k \nu_{kj,f} r_{k,f} + \sum_k \nu_{kj,b} r_{k,b} \tag{17}$$

The second term on the righthand side of Eq. 17 is a linear function of the concentration of component j in the ith gridpoint of a section, neglecting the small contribution of possible recombination reactions. Equation 17 can then be rewritten

$$\sum_k \nu_{kj} r_k = \sum_k \nu_{kj,f} r_{k,f} + KC_{j,i} \tag{18}$$

Separation of the righthand side of Eq. 16 according to Eq. 18 by moving the second term on the righthand side to the left side of Eq. 16 solves the stiffness problem. The diagonal elements of the tridiagonal matrix increase; hence, the stability of the solution is increased.

Simulation conditions

An industrial ethane-cracking furnace is simulated. The energy required for the steam cracking of the ethane feed is provided by radiation burners. An identical heat-flux profile is used as input, to have a good basis for the comparison of the results obtained with both reactor models. Hence, the same amount of energy is added to the process gas. The heat-flux profile was obtained by performing a coupled simulation of the furnace and the reactor tubes, using the 1-D reactor model. For the calculation of the furnace the zone method of Hottel and Sarofim (1967) is used. This simulation method is developed by Vercammen and Froment (1980), Rao et al. (1988), and Plehiers and Froment (1989).

The furnace is divided into a number of isothermal surface and volume zones. The energy balances, containing radiative, convective, and conductive contributions, are constructed for these zones. Furnace-wall, process-gas, and tube-skin temperature profiles in the furnace are obtained by solving the energy balances. From these temperature profiles, a better estimate of the heat-flux profile is obtained, based on which a new reactor calculation is performed. With the resulting tube-skin temperature profile, a new furnace calculation is performed. This cycle is repeated until convergence is reached.

For the simulated ethane-cracking furnace, the burners are located in the sidewalls on both sides of the coils. The flue gas entering the furnace through the burners delivers energy to the reactor wall and therefore decreases in temperature. The flue gas temperature is higher in the bottom section of the furnace due to the hampered flow. In the top section there are no burners, so the flue-gas temperature profile is smoother. The nonuniformity of the flue-gas temperature results in a strongly varying heat flux to the process gas, as shown in Figure 1. At the top of the furnace the heat flux is much lower than at the bottom where there are sharp peaks.

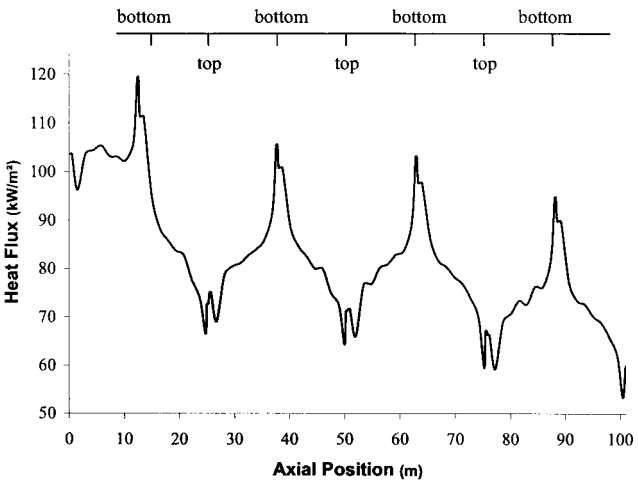

Figure 1. Heat flux from furnace to reactor as a function of axial position in the reactor coil.

There was no coupled simulation of furnace and reactor coils performed using the 2-D reactor model. For reasons of comparison, as explained earlier, the same heat-flux profile was used. However, the slight change in the external tube-skin temperature profile will result in a small change in the heat-flux profile when a complete simulation is performed. The operating conditions and the furnace and reactor geometry are listed in Table 1. The total hydrocarbon flow rate through one reactor coil is 3.5 tons per hour. The inlet temperature of the process gas is 873 K. During the steam cracking of ethane a steam dilution of 0.35 kg per kg feed is applied. The steam reduces the partial pressure of the hydrocarbons in the gas phase and reduces the coke formation.

Results and Discussion

The cracking of ethane has been simulated with a 1-D and a 2-D reactor model. For the 2-D simulation, this results in important radial nonuniformities of the temperature in the reactor coil, as shown in Figure 2. The radial temperature

Table 1. Furnace, Reactor Geometry, and Process Conditions for the Standard Ethane Cracking Furnace.*

Furnace	
Furnace length	9.30 m
Furnace height	13.45 m
Furnace width	2.10 m
Thickness refractor material	0.23 m
Thickness insulation material	0.05 m
Number of burners	128
Heat input	14.43 MW
Reactor coil	
Number of reactors	4
Number of passes	8
Reactor length	100.96 m
Reactor diameter (int)	0.124 m
Wall thickness	0.008 m
Ethane flow rate per reactor coil	0.972 kg s^{-1}
Steam dilution	0.35 kg/kg
CIT*	873 K
CIP**	0.34 MPa

*Coil inlet temperature.
**Coil inlet pressure.

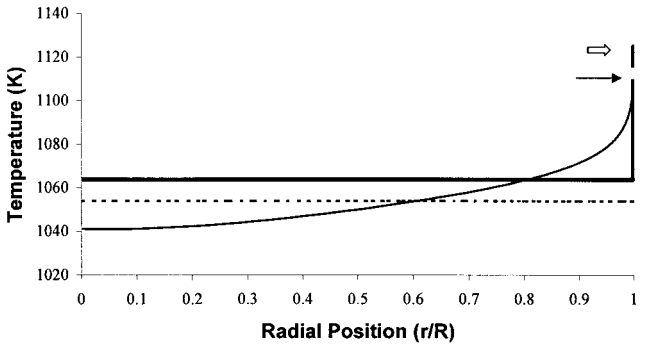

Figure 2. Process-gas temperature in function of radial position at an axial position of 50 m.

– 1-D reactor model; — 2-D reactor model; - -- - average 2-D; ⇐ internal-wall-temperature 1-D reactor model; ← internal-wall-temperature 2-D reactor model.

profile simulated with the 2-D model shows a strong gradient near the wall, but the gradients in the center of the tube cannot be neglected, in contrast to the 1-D model. The total temperature drop from the wall to the center is about 100 K for both models. Figure 2 also shows the average process gas temperature for the 2-D simulation. The cup-mixing temperature is applied for the calculation of the average process-gas temperature for the 2-D reactor model (Bird et al., 2001)

$$T_{av} = \frac{\int_0^R T(r)u(r)r\,dr}{\int_0^R u(r)r\,dr} \tag{19}$$

The results of Figure 2 are in agreement with the results simulated by Froment (1992), who reported a similar radial temperature profile, but with a stronger temperature drop near the wall, for a pilot configuration with a reactor tube diameter of 0.037 m and, hence, a lower velocity.

In Figure 3 the axial profiles of the average process-gas temperatures and the wall temperatures for the two simulation models in the reactor coil are given. Although important differences exist for the temperature in a radial section, there is good agreement between the average gas temperature calculated with the 2-D reactor model and the gas temperature simulated with the 1-D reactor model up to 25 m. From this position the cracking becomes significant and is more pronounced when the radial temperature profiles are accounted for. This leads to an average temperature that is lower for the 2-D model.

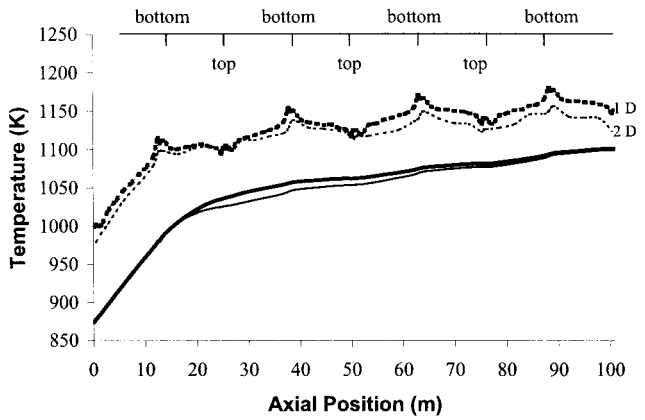

Figure 3. Average process-gas temperature and internal tube-skin temperature as a function of axial position in the reactor coil.

– Process-gas temperature 1-D; — average process-gas temperature 2-D; – – – tube-skin temperature 1-D; --- tube-skin temperature 2-D.

Table 2. Composition Between Simulated wt. % at the Reactor Outlet of the Traditional Single Coil Reactor Simulated with the 1-D and 2-D Reactor Model

	1-Dimensional	2-Dimensional
H_2	3.15	3.04
CH_4	2.85	4.73
C_2H_2	0.39	0.27
C_2H_4	41.44	40.75
C_2H_6	49.00	47.75
C_3H_6	0.74	1.31
C_4H_6	0.89	1.10
C_4H_8	0.17	0.20

The wall temperature for the 1-D simulation is slightly higher than the one simulated with the 2-D reactor model. This is due to the different calculation methods used for the wall temperatures. The Dittus-Boelter equation and the gas temperature are used in the 1-D model (see Eq. 3), while in the 2-D model heat transport and reaction are considered simultaneously (see Eq. 6). The latter implies a better simulation of the wall temperature. The higher wall temperature resulting from the 1-dimensional reactor model will have consequences for coke formation. Higher temperatures in the zone near the wall will increase the simulated coking rate.

Effect of the radial temperature profile on product distribution and conversion

The radial temperature profile has a large influence on the simulated product yields and the conversion. The weight fractions at the outlet of the reactor are given in Table 2. Except for hydrogen, the differences cannot be neglected. Especially for methane and propylene the yields calculated with the 2-D model are much higher. On the other hand, for acetylene and ethylene the 2-D model simulates a lower product yield.

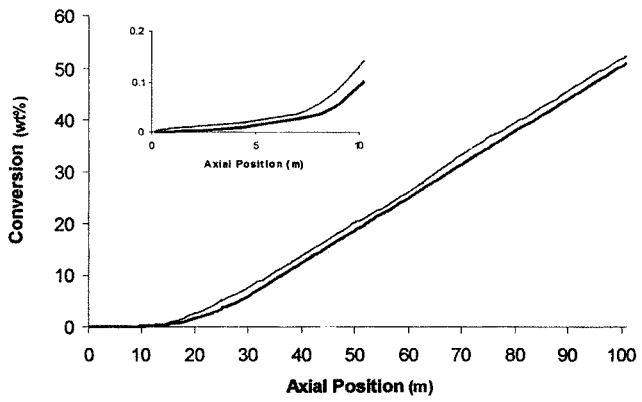

Figure 4. Ethane conversion as a function of axial position in the reactor coil.

– 1-D reactor reactor model; — 2-D reactor model.

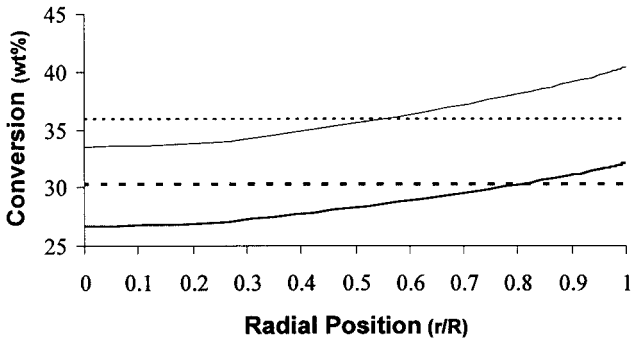

Figure 5. Conversion and ethylene yield as a function of radial position at an axial position of 75 m.

– Ethylene yield 2-D; – – – ethylene yield 1-D; — ethane conversion 2-D; - - - - - ethane conversion 1-D.

The existence of an important radial temperature profile is the main cause for the differences in product distribution obtained with both reactor models. The interpretation of radial and axial concentration profiles of the most important molecules and radicals, taking into account the radial and axial temperature profiles, will allow this to be explained. The main molecules in the kinetic model for the cracking of ethane are ethane, ethylene, propylene, and hydrogen. The main radicals are the hydrogen, methyl, ethyl, and allyl radicals.

Ethane Conversion. The ethane conversion profile is shown in Figure 4. Such a profile shows an induction period corresponding with the heating of the process gases to the reaction temperature. This induction period is shorter for the 2-D model because of the radial temperature profile. Figure 3 shows that in the zone near the wall the temperature is more than 60 K higher than the average temperature and, hence, activation by C–C scission or C–H scission reactions will occur at an axial position closer to the inlet. This effect results in a higher ethane conversion obtained with the 2-D reactor model. At temperatures below 1100 K, the C–C scission of ethane with an activation energy of 368 kJ/mol is the main source of methyl radicals

$$C_2H_6 \rightarrow CH_3\cdot + CH_3\cdot \tag{20}$$

The C–H scission reactions only become of some importance at much higher temperatures, because of the higher activation energy of this reaction (411 kJ/mol). The influence of the small difference between the average process-gas temperature simulated with the 2-D model and the 1-D temperature is of less importance. Once the cracking has started, the conversion of ethane increases with an almost constant slope.

In Figure 5 the ethane conversion and the ethylene yield are shown over a cross section at an axial position of 75 m. The radial temperature profile is responsible for the radial differences in conversion. The higher conversion near the wall results in a higher ethylene yield in this zone. The higher conversion in this zone will also affect the yields of other products.

Product Yields. As shown in Table 2, the methane yield simulated with the 2-D reactor model is higher than simulated with the 1-D reactor model. As a consequence of the radial temperature profile and the resulting increase of C–C scission reactions of ethane, a higher methyl radical concentration is obtained. H-abstraction reactions by the methyl radical lead to the formation of methane. In this case, the H-abstraction reaction of ethane is the main path to the formation of methane

$$CH_3\cdot + C_2H_6 \rightarrow CH_4 + C_2H_5\cdot \tag{21}$$

The higher methane yield at the outlet is thus a direct consequence of the higher methyl radical concentration.

The lower ethylene yield simulated at the reactor outlet with the 2-D reactor model is due to diffusional effects. Near the inlet of the reactor only the process gas temperature in the zone near the wall is high enough to activate the conversion of ethane. Decomposition of the ethyl radical is generally accepted to be the main reaction responsible for the production of ethylene from ethane

$$C_2H_5\cdot \rightarrow C_2H_4 + H\cdot \tag{22}$$

The ethylene produced in the zone near the wall can diffuse to the center of the tube where the temperatures are lower. These temperatures favor secondary reactions, among which addition reactions to methyl and ethyl radicals are very important

$$CH_3\cdot + C_2H_4 \rightarrow C_3H_7\cdot \tag{23}$$

$$C_2H_5\cdot + C_2H_4 \rightarrow C_4H_9\cdot \tag{24}$$

This explains the higher yield of products such as propylene, 1-butene, and butadiene, obtained with the 2-D reactor model. For example, propylene is mainly formed by the β-scission of the $C_3H^{\bullet}$-radical

$$C_3H_7\cdot \rightarrow C_3H_6 + H\cdot \tag{25}$$

and in a small amount from H-abstraction reactions by the allylic $C_3H_5^{\bullet}$ radical:

$$C_3H_5\cdot(al) + C_2H_6 \rightarrow C_3H_6 + C_2H_5\cdot \tag{26}$$

Diffusion of ethylene, followed by addition of the methyl radical (Eq. 23) results in higher propylene formation.

The same reasoning that explains the lower ethylene yield also holds for the lower acetylene yield obtained with the 2-D reactor model. Diffusion of acetylene to the center, followed by

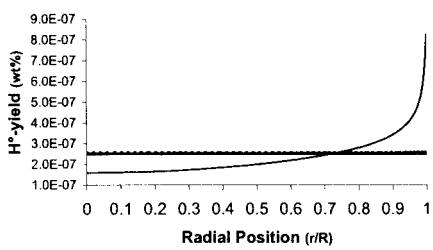

Figure 6. Simulated weight-fraction profiles for the H radical at an axial position of 75 m.

– 1-D; — 2-D; - - - - average 2-D.

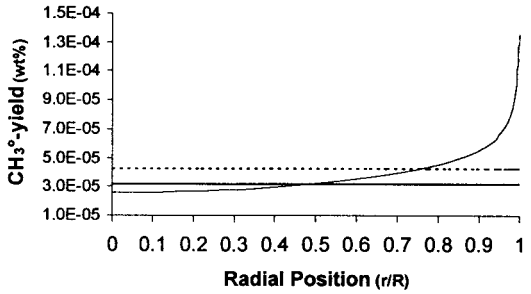

Figure 7. Simulated weight-fraction profiles for the CH_3 radical at an axial position of 75 m.

– 1-D; — 2-D; - - - - average 2-D.

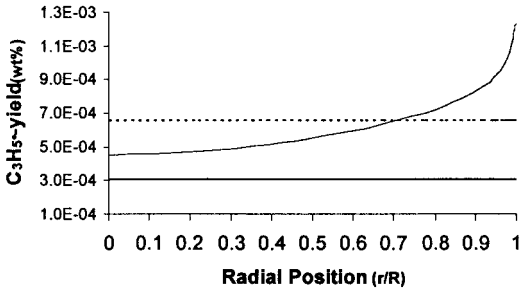

Figure 9. Simulated weight-fraction profiles for the allylic C_3H_5 radical at an axial position of 75 m.

– 1-D; — 2-D; - - - - average 2-D.

secondary reactions, explains the lower acetylene yield. The effect is even more pronounced due to the faster secondary acetylene reactions, which decrease the acetylene yield drastically in favor of heavier products.

Radical Concentration Profiles. The radial yield profiles for the main radicals are presented in Figures 6 to 9. Comparing these profiles with those in Figure 5 for ethylene and ethane, it is clear that the radial gradient for the radicals is much steeper than for the molecular species. The radial temperature profile results in strong radial gradients for the radicals, especially for the methyl radical and the hydrogen radical.

The combined effects of the radial temperature profile and the resulting radial yield profile for the methyl radical are the main cause for the radial nonuniformities for the heavier radicals and for the higher average radical concentration simulated with the 2-D reactor model (Figures 8 and 9). The radial average yield of the allylic radical is about two times higher when using the 2-D reactor model, and that of the methyl radical is almost 1.5 times higher. The latter is in contrast with the results for the hydrogen radical in Figure 6. The average H-radical yield simulated with the 2-D reactor model is slightly lower than the one simulated with the 1-D reactor model. The lower H_2 yield simulated with the 2-D reactor model in Table 2 also suggests that fewer H-abstractions by H-radicals occur. This is due to the high activation energy of the C–H scission reaction of ethane

$$C_2H_6 \rightarrow C_2H_5\cdot + H\cdot \qquad (27)$$

The temperatures are high enough to activate this reaction (Eq. 27) and increase the H-radical concentration drastically only in a small zone near the wall. This zone, however, is much smaller than the one observed for the formation of the methyl radical through Eq. 20. Taking into account the lower average temperature obtained with the 2-D reactor model, a global lower average H-radical yield is simulated.

Effect of Tube Diameter. The existence of the radial temperature profile in a tubular reactor clearly has a strong influence on the product yields. For a given average temperature, the presence of a radial temperature profile leads to a decrease of the yield of ethylene. This implies that tubes with a smaller diameter are beneficial because of a stronger 1-D behavior. This is the case for reactor configurations such as the USC-Furnace (Ultra Selective Conversion) developed by Stone and Webster, and the Kellogg Millisecond Furnace. Consider, for example, the Kellogg Millisecond Furnace. This type of furnace, consisting of a reactor with a large number of tubes (200) of small diameter ($3.5 \cdot 10^{-2}$ m) and short length (10 m) (Orriss and Yamaguchi, 1987), is known for its high ethylene yield. The total hydrocarbon flow rate of more than 20 ton per h results in very high velocities in all of 200 parallel tubes. The high yield in ethylene of this type of reactor is generally explained by the short residence time. Indeed, short residence times reduce the disappearance of light olefins because of secondary reactions such as addition reactions. Experimental work by Ennis et al. (1975) showed that residence times lower than 0.1 s are most favorable. The results in this article indicate that not only the short residence time but also a stronger 1-D behavior is the cause for the high ethylene yield.

The simulation conditions for one of 200 tubes of a standard

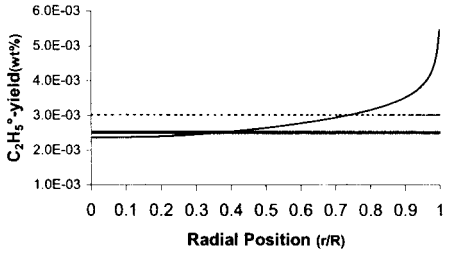

Figure 8. Simulated weight-fraction profiles for the C_2H_5 radical at an axial position of 75 m.

– 1-D; — 2-D; - - - - average 2-D.

Table 3. Calculated Temperature (K) and Concentration ($kmol \cdot m^{-3}$) of the Main Coke Precursors at the Gas–Coke Interface (z = 50 m).

	1-Dimensional		
	Process Gas	Interface	2-D
T	1125	1125	1120
C_2H_2	$6.26 \cdot 10^{-6}$	$6.71 \cdot 10^{-6}$	$6.28 \cdot 10^{-6}$
C_2H_4	$3.66 \cdot 10^{-3}$	$3.53 \cdot 10^{-3}$	$3.67 \cdot 10^{-3}$
C_3H_4	$1.25 \cdot 10^{-7}$	$1.26 \cdot 10^{-7}$	$1.56 \cdot 10^{-7}$
C_3H_6	$1.67 \cdot 10^{-5}$	$3.64 \cdot 10^{-5}$	$4.28 \cdot 10^{-5}$
$H^{\cdot}$	$9.76 \cdot 10^{-10}$	$7.57 \cdot 10^{-9}$	$3.61 \cdot 10^{-9}$
$CH_3^{\cdot}$	$6.37 \cdot 10^{-9}$	$4.82 \cdot 10^{-8}$	$3.96 \cdot 10^{-8}$
$C_2H_5^{\cdot}$	$4.43 \cdot 10^{-7}$	$1.20 \cdot 10^{-6}$	$1.15 \cdot 10^{-6}$
$C_3H_5^{\cdot}$	$1.26 \cdot 10^{-8}$	$7.20 \cdot 10^{-7}$	$8.80 \cdot 10^{-8}$

Note: 1-D reactor model, precursor concentrations calculated at process-gas temperature; 1-D reactor model, precursor concentrations calculated at interface temperature; 2-D reactor model, precursor concentrations at interface.

Table 4. Reactor Geometry and Process Conditions for the Reactor Configuration in a Millisecond Furnace

Reactor diameter (int)	0.035 m
Wall thickness	0.008 m
Total ethane flow rate	0.972 kg s^{-1}
Number of reactor tubes	150
Steam dilution	0.35 kg/kg
CIT*	873 K
CIP**	0.20 MPa

Position (m)	Heat flux (kJ · m^{-2} s^{-1})
0.00	125.9
0.50	125.3
1.29	117.1
2.08	112.3
3.66	107.3
5.25	101.5
6.83	93.6
8.41	80.2
10.00	73.8

*Coil inlet temperature.
**Coil inlet pressure.

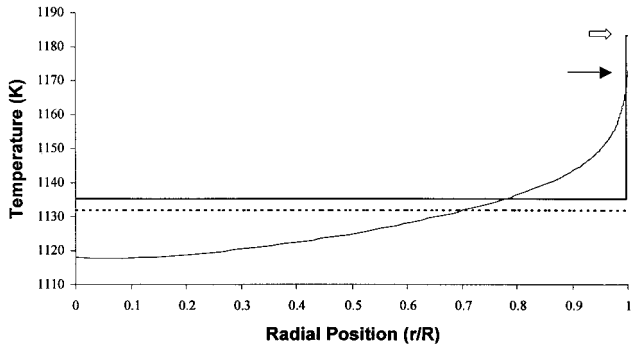

Figure 10. Process-gas temperature in function of radial position at an axial position of 6.7 m for a tube of the Milliesecond Furnace

– 1-D reactor model; — 2-D reactor model; - - - - average 2-D, ⇐ internal-wall-temperature 1-D reactor model; ← internal-wall-temperature 2-D reactor model.

Millisecond Furnace configuration are summarized in Table 4. They have been chosen in order to obtain an ethane conversion similar to those just discussed. The simulation results in Table 5 show that the difference between the 1-D reactor model and the 2-D reactor model are significantly smaller than for the traditional single coil reactor, but cannot be neglected. The main reason for the differences is again the radial temperature profile, but the stronger 1-dimensional behavior reduces the radial nonuniformities. A radial temperature profile for one of the tubes of the Kellogg Millisecond Furnace is shown in Figure 10. The high velocities through the small-diameter tube reduce the total temperature drop from the wall to the center to 55 K, which is significantly smaller than for the traditional single coil.

In industry the Kellogg Millisecond Furnace is operated under much more severe conditions. The high heat fluxes necessary to achieve these high conversions lead to more pronounced temperature gradients, and hence to stronger effects on the yields than under the simulation conditions in Table 4. Therefore rifled tubes are used in industry (Orriss and Yamaguchi, 1987), as they promote heat transfer by means of their spirally grooved internal surface, reducing the radial temperature profile.

Effect of the radial temperature profile on coke formation

The coke formation at the internal skin of the reactor coil depends on the conditions prevailing at the process gas–coke interface. It is clear from the preceding results obtained with the 2-D reactor model that these conditions differ appreciably from the process conditions at the center of the reactor coil. In typical industrial units, the temperature at the interface can be up to 100 K higher than the average process gas temperature. This has a significant effect on the gas-phase concentrations, particularly on those of the gas phase radicals. According to Reyniers et al. (1994), gas-phase radicals generate radical sites on the cokes layer. Olefins can add to these radical sites after dehydrogenation coke is formed. Therefore the effect of the radial temperature profile and the resulting gas-phase radical concentration profile on the coking rate has been investigated for a traditional single-coil reactor. The simulation results using a fundamental kinetic coking model based on elementary reactions are studied. These results are compared with reference data calculated with the model of Plehiers (1989). The coking model of Plehiers (1989), coupled to a 1-D reactor model, has been validated for experimental as well as industrial units and was found to be very useful for the prediction of coke formation in the steam cracking of light hydrocarbon feedstocks. The run length of several industrial cracking units has been simulated, showing a good agreement between industrial and simulated results. An agreement of results obtained with the coking model based on elementary reactions on the one hand, and those obtained with the coking model of Plehiers on the other hand, is therefore a good indication for the quality of the simulation results discussed in this article. The semiempirical coking model of Plehiers considers ethylene and propylene to be the only coke precursors. These components can add to the radical sites at the coke surface and form cokes. The coking rate is a function of the wall temperature and the concentration of ethylene and propylene.

A fundamental kinetic model for coke formation based on elementary reactions has been developed for the cracking of light feedstocks by Wauters and Marin (2001). The creation of radical sites on the coke layer is explicitly accounted for by considering the abstraction of hydrogen from surface species by gas-phase radicals. The resulting radical surface species can add to unsaturated components, such as olefins and aromatics, in the gas phase. The possible coke-formation reactions can be divided into five classes:

Table 5. Comparison Between Simulated Weight Percentages (%) at the Reactor Outlet for the 1-D and 2-D Reactor Model for One Tube of a Millescond Furnace

	1-Dimensional	2-Dimensional
H_2	3.21	3.16
CH_4	2.24	3.09
C_2H_2	0.40	0.34
C_2H_4	42.27	41.97
C_2H_6	49.47	48.75
C_3H_6	0.46	0.61
C_4H_6	0.78	0.84
C_4H_8	0.11	0.13

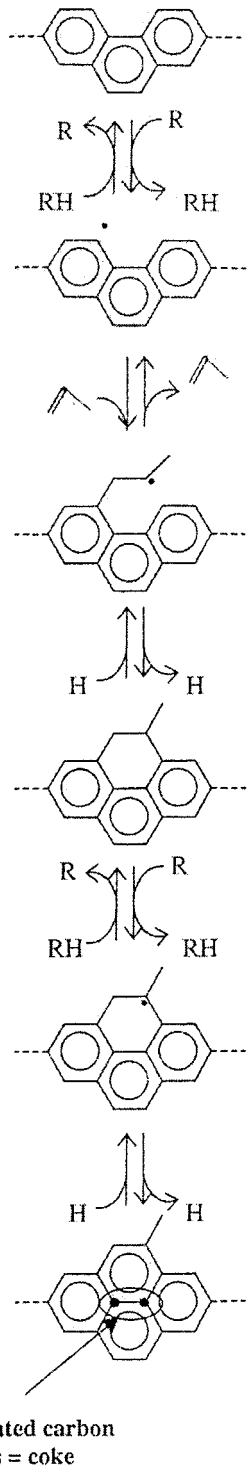

Figure 11. Reaction path for coke formation starting from propylene, hydrogen radicals, and alkyl radicals; the coke layer is considered to be a polyaromatic surface

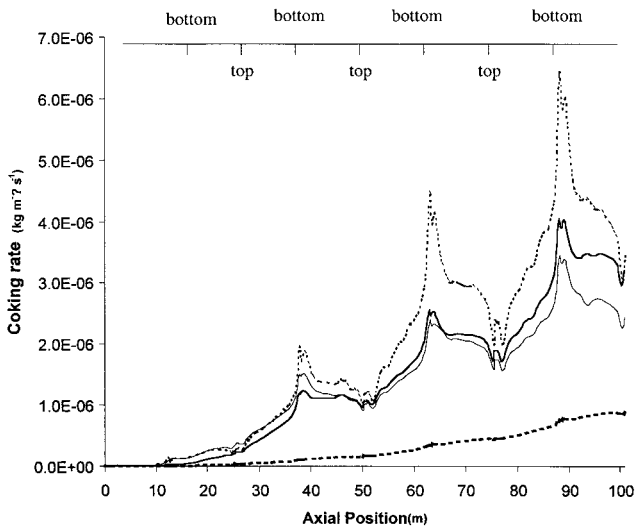

Figure 12. Coking rate as a function of axial position in the reactor tube.

– Reference profile; ––– 1-D reactor model, precursor concentrations calculated at process gas temperature; - - - 1-D reactor model, precursor concentrations calculated at interface temperature; — 2-D reactor model, precursor concentrations at interface.

- Hydrogen abstraction by gas-phase radicals;
- Substitution by gas-phase radicals at the coke surface;
- Addition of a radical surface species to a gas-phase olefin and the reverse decomposition of a radical surface species in a smaller radical surface species and an olefin;
- Addition of a gas-phase radical to a double bond in a surface species and the reverse decomposition of a radical surface species to an olefinic surface species and a radical;
- Cyclization of a radical surface species and decyclization.

Figure 11 shows one of the reaction paths for coke-layer growth starting from propylene, hydrogen radicals, and alkyl radicals as coke precursors. The coke layer is considered to be a polyaromatic surface.

Considering each component in such a coke-formation model leads to an enormous expansion of the reaction network. To obtain a rigorous but practical model, it is, therefore, necessary to select those gas-phase components that are the most important coke precursors. The contribution of a gas-phase component to the coke formation is determined by the concentration of the component and the rate coefficients of the coking reactions in which the component is involved. In steam cracking of light feedstocks the concentration of the gas-phase radicals varies between 10^{-6} mol m^{-3} and 10^{-1} mol m^{-3} (McConnell et al., 1981). The latter was confirmed by the simulation results. For light feedstocks, the hydrogen, methyl, ethyl, and allyl radicals were found to be the most important coke precursor radicals. Acetylene, ethylene, methylacetylene, and propylene are unsaturated molecular components that favor coke formation.

The kinetics of the coke-formation reactions are determined from those of corresponding gas-phase reactions, provided the presence of a solid phase is accounted for via a correction factor based on the collision theory (Wauters and Marin, 2002). It was found that the coking rate depends not only on the concentration of molecules and on the wall temperature, but in

particular on the radical concentrations. A good estimation of the concentrations of the radicals in the zone near the wall is of the utmost importance for the fundamental coking model, because their effect on the coking rate is as important as the effect of the wall temperature (Wauters and Marin, 2002).

In Figure 12, the differences between the coking-rate profiles calculated with the 1-D and 2-D reactor model, are presented and compared with the reference profile. Using a 1-D reactor model and calculating the precursor concentrations at the process-gas temperature clearly underestimates the coking rate. The wall temperature used in this simulation is the wall temperature calculated with the 1-D reactor model. The reason for the large difference between the calculated profile and the reference profile is twofold. On the one hand, the effect of the temperature for the calculation of the coking rate with the fundamental model is not as strongly affected by the temperature as the calculation of the coking rate calculated with the semiempirical model (Wauters and Marin, 2002), that is, the reference profile, due to differences in kinetics. On the other hand, the precursor concentrations are those calculated in the process gas by the 1-D reactor simulation. Table 3 shows the values of the concentrations of the main coke precursors and the temperature at $z = 50$ m. The concentrations calculated in the process gas with the 1-D reactor simulation are lower than those prevailing at the interface as calculated with the 2-D reactor model. The underestimation of the concentrations of the species result in a drastic underestimation of the coking rate. For example the underestimation of the methyl radical by a factor of 5 results in a reduction of the coking rate by almost 50% (Wauters and Marin, 2002).

As an approximation, the concentrations of the coke precursors at the interface temperature have been calculated by solving the corresponding mass balances for the 1-D reactor model but now at the interface temperature. The agreement between the simulated profile and the reference profile is improved, but the coking rate is now overestimated. A higher temperature increases the precursor concentrations as compared to those calculated with the 2-D model (see Table 3) and causes the overestimation of the coking rate.

As shown in Figure 12 the coking-rate profile calculated with the coking model based on elementary reactions and using the 2-D reactor model shows good agreement with the reference profile obtained from the semiempirical model of Plehiers (1989). The coke-formation profile calculated with the model based on elementary reactions coupled to the 1-D reactor model shows only small peaks, if any, at the higher tube-wall temperatures. On the other hand, when coupled to the 2-D reactor model the sharp peaks obtained for the coking-rate profile calculated with the model of Plehiers are almost perfectly predicted. The peaks simulated with the latter are a direct consequence of the peaks in the tube-wall temperature profile (Figure 2). This reasoning does not hold for the coking-rate profile simulated with the fundamental coking model and the 2-D reactor model. Here, the effect of the interface temperature on the coke precursor concentrations is incorporated via the kinetics and the concentrations of the involved reactants, in particular of the radicals. Hence, the coke precursor concentrations need to be calculated at the interface temperature. The latter can only be calculated accurately with a 2-D reactor model. The simulation results clearly show the potential of this fundamental model coupled to a 2-D reactor model and shows the importance of applying a more-dimensional reactor model.

Conclusions

Comparison of the simulation results using a 1-dimensional and a 2-D reactor model for ethane steam cracking indicates that important radial gradients exist, not only for the temperature but also for the molecular and in particular the radical species. The effect of the radial temperature profile on the concentration profiles and on the reaction rates of the elementary reactions considered by the kinetic cracking model makes it possible to explain the differences in simulated product yields for the two reactor models. The radial temperature profile decreases the yield for ethylene because light olefins are removed by secondary reactions, generating species with higher molecular weight such as propylene and butadiene. As a corollary this, it can also be concluded that reactors with a stronger 1-D character allow a higher ethylene yield to be obtained. This was illustrated for the reactor configuration of a Kellogg Millisecond Furnace.

The simulation results obtained with a fundamental kinetic coking model based on elementary reactions have been investigated. These results have been compared with the reference data of a validated semiempirical model. The coupling of a fundamental coke-formation model based on elementary reactions to a 1-D reactor model was found to result in large disparities compared to the reference data, mainly due to deviations in the simulated concentrations of the coke precursors. A 2-D reactor model allows us to adequately account for the coke precursor concentrations and, hence, to properly simulate the coking rates in an industrial ethane steam-cracker.

The differences noticed for both the product yields and the coking rate exceed the degree of accuracy required today. Therefore, the use of a 2-D reactor model is necessary, even if this increases the computational effort.

Acknowledgments

The authors are grateful to the "Fonds voor Wetenschappelijk Onderzoek-Vlaanderen" and Technip-Benelux for financial support of the steam-cracking research. Kevin M. Van Geem holds a PhD grant of the Institute for the Promotion of Innovation by Science and Technology in Flanders (IWT-Vlaanderen).

Notation

C_j = concentration of component j, kmol · m^{-3}
$c_{p,j}$ = heat capacity of component j, kJ · kmol^{-1} K^{-1}
D_m = molecular diffusion coefficient, m^2 s^{-1}
d_t = internal tube diameter, m
f = Fanning friction factor
F_j = molar flow rate, kmol · s^{-1}
G = mass flux, kg · m^{-2} s^{-1}
H = enthalpy of the process gas, kJ · kmol^{-1}
H_j = enthalpy of formation of component, j, kJ · kmol^{-1}
ΔH_k = heat of reaction k, kJ · kmol^{-1}
M_j = molecular weight of component j, kg · kmol^{-1}
n = number of grid points
n_{ij} = number of reactions in which i and j participate
Nu = Nusselt number
p_t = total pressure, MPa
q = heat flux, kJ · m^{-2} s^{-1}
r = radial coordinate, m
r_b = radius of the bend, m
Pr = Prandtl number

R = radius of the bend, m
$R_{k,j}$ = rate of reaction k in which j participates, kmol · m^{-3} s^{-1}
r_{cj} = coking rate of reaction in which j participates, kg · m^{-2}_{react} s^{-1}
Re = Reynolds number
Sc = Schmidt number
T = process-gas temperature, K
u = velocity of the process gas, ms^{-1}
w_j = weight fraction of j in the process-gas mixture
x = normalized radial position
z = axial coordinate, m

Greek letters

α = conversion factor depending on the units of p_t
δ = steam to hydrocarbon dilution
ϵ = distance to the wall, m
ϵ_H = turbulent conduction coefficient, kJ · s^{-1} · m^{-1} K^{-1}
ϵ_D = turbulent diffusion coefficient, m^2 s^{-1}
λ_m = thermal conduction coefficient, kJ · m^{-1} s^{-1}
ζ = Nekrasov factor for bends
Ω = cross section, m^2
ρ_g = density of the process-gas mixture, kg · m^{-3}
τ_w = shear stress, kg · s^{-2} · m^{-1}
ω = wetted perimeter of the tube, m
ν = kinematic viscosity, m^2 s^{-1}
v_{kj} = stoechiometric coefficient of the component j in the reaction k

Subscripts and superscripts

b = backward
f = forward
i = grid point in a radial section
j = component
r = radial
z = axial
av = average

Literature Cited

Bird, R. B., E. N. Lightfood, and W. E. Stewart, *Transport Phenomena,* Wiley, New York (2001).

Clymans, P. J., and G. F. Froment, "Computer Generation of Reaction Paths and Rate Equations in the Thermal Cracking of Normal and Branched Paraffins," *Comp. Chem. Eng.,* **8,** 137 (1984).

Davies, J. T., *Turbulence Phenomena,* Academic Press, London (1972).

Dente, M., and E. Ranzi, "Detailed Prediction of Olefin Yields from Hydrocarbon Pyrolysis Through a Fundamental Simulation Program (SPYRO)," *Comp. Chem. Eng.,* **3,** 61 (1979).

De Saegher, J. J., T. Detemmerman, and G. F. Froment, "Three Dimensional Simulation of High Severity Internally Finned Cracking Coils for Olefins Production," *Rev. de Inst. Fr. Pet.,* **51,** 246 (1996).

Ennis, B. P., H. B. Boyd, and R. Orriss, "Olefin Manufacture via Millisecond Pyrolysis," *Chemtech,* **5**(11), 693 (1975).

Fagley, J. C., "Simulation of Transport in Laminar, Tubular Reactors and Application to Ethane Pyrolysis," *Ind. Eng. Chem. Res.,* **31,** 58 (1992).

Froment, G. F., and K. B. Bishoff, *Chemical Reactor Design and Analysis,* Wiley, New York (1990).

Froment, G. F., "Kinetics and Reactor Design in the Thermal Cracking for Olefin Production," *Chem. Eng. Sci.,* **47,** 2163 (1992).

Heynderickx, G. J., C. C. Cornelis, and G. F. Froment, "Circumferential Tube Skin Temperature Profiles in Thermal Cracking Coils," *AIChE J.,* **38,** 1905 (1992).

Heynderickx, G. J., and G. F. Froment, "Simulation and Comparison of the Run Length of an Ethane Cracking Furnace with Reactor Tubes of Circular and Elliptical Cross Sections," *Ind. Eng. Chem. Res.,* **37,** 914 (1998).

Hottel, H. C., and A. F. Sarofim, *Radiative Transfer,* McGraw-Hill, New York (1967).

McConnell, C. F., and B. D. Head, "Pyrolysis of Ethane and Propane," *Pyrolysis*, Academic Press, New York (1981).

Orriss, R., and H. Yamaguchi, "Idemitsu's Chiba Ethylene Plant Proves Modern Technology," *Oil & Gas J.,* **9,** 27 (1987).

Plehiers, P. M., "Rigoureuze Modellen voor de Simulatie van Fornuizen voor de Thermische Kraking van Lichte Koolwaterstoffen," PhD Thesis, Ghent Univ., Ghent, Belgium (1989).

Plehiers, P. M., and G. F. Froment, "The Uno-Quattro Coil: High Severities for Increased Ethylene Selectivity," *Ind. Eng. Chem. Res.,* **30,** 1081 (1991).

Plehiers, P. M., and G. F. Froment, "Firebox Simulation of Olefin Units," *Chem. Eng. Commun.,* **80,** 81 (1989).

Rao, M. V. R., P. M. Plehiers, and G. F. Froment, "The Coupled Simulation of Heat Transfer and Reaction in a Pyrolysis Furnace," *Chem. Eng. Sci.,* **43,** 1222 (1988).

Reyniers, G. C., G. F. Froment, F. D. Kopinke, and G. Zimmerman, "Coke Formation in the Thermal Cracking of Hydrocarbons. 4. Modeling of Coke Formation in Naphtha Cracking," *Ind. Eng. Chem. Res.,* **33,** 2584 (1994).

Sundaram, K. M., "Kinetic Modeling of Thermal Cracking as a Basis for Reactor Simulation," PhD Thesis, Ghent Univ., Ghent, Belgium (1977).

Sundaram, K. M., and G. F. Froment, "2 Dimensional Model for the Simulation of Tubular Reactors for Thermal Cracking," *Chem. Eng. Sci.,* **35,** 364 (1980).

Sundaram, K. M., and G. F. Froment, "Comparison of Simulation Models for Empty Tubular Reactors," *Chem. Eng. Sci.,* **34,** 117 (1979).

Sundaram, K. M., P. S. Van Damme, and G. F. Froment, "Coke Deposition in the Thermal Cracking of Ethane," *AIChE J.,* **27,** 946 (1981).

Valenyi, L. J., Y. Song, and J. C. Fagley, "Carbon Deposition in Ethane Pyrolysis Reactors," *Ind. Eng. Chem. Res.,* **30,** 1078 (1991).

Vercammen, H. A. J., and G. F. Froment, "An Improved Zone Method for the Simulation of Radiation in Industrial Furnaces," *Int. J. Heat Transfer,* **23**(3), 329 (1980).

Wauters, S., and G. B. Marin, "Computer Generation of a Network of Elementary Steps for Coke Formation During the Thermal Cracking of Hydrocarbons," *Chem. Eng. J.,* **82,** 267 (2001).

Wauters, S., and G. B. Marin, "Kinetic Modeling of Coke Formation during Steam Cracking," *Ind. Eng. Chem. Res.,* **41,** 2379 (2002).

Manuscript received Nov. 16, 2002, and revision received May 12, 2003.